Supporting Online Material for

Single Molecule Lysozyme Dynamics Monitored by an Electronic Circuit

Yongki Choi, Issa S. Moody, Patrick C. Sims, Steven R. Hunt, Brad L. Corso, Israel Perez, Gregory A. Weiss*, and Philip G. Collins*

correspondence to: *gweiss@uci.edu* or *collinsp@uci.edu*

This PDF file includes:

A-1. Lysozyme mutagenesis.

The T4 lysozyme variants applied here were based upon the pseudo-wild-type variant of T4 lysozyme with the substitutions C54T C97A (a generous gift from Prof. Brian Matthews, University of Oregon). An ORF encoding this pseudo-wild-type T4 lysozyme, hereafter referred to as lysozyme, provided a template for splice overlap extension PCR, using the primers P1-For, P2-RevSC90, P3-ForSC90, and P4-Rev listed in Table S1. The amplicon encoding the S90C lysozyme variant was subcloned into the pET28 vector for protein overexpression.

The gene encoding the T26E/C54T/S90C/C97A variant of lysozyme (hereafter termed the T26E variant of lysozyme) used similar protocols and the primers P1-For, P2-RevT26E, P3-ForT26E, and P4-Rev6xH (Table S1); this construct, unlike the other reported lysozyme variants, also included a His_6 epitope and TEV protease site at the C-terminus, which was prone to proteolysis. The additional sequence was not expected to affect the results from this control protein; the protein remained inactive as reported and also in ensemble measurements as previously reported (*41, 58*).

The gene encoding the E11H/C54T/C97A variant of lysozyme (hereafter termed the E11H variant of lysozyme) was synthesized by similar protocols and the primers E11H-For, E11H-Rev, P1-For-NCys and P4-Rev (Table S1); this gene also encoded an inserted cysteine near the N-terminus to provide a reactive thiol for bioconjugation. The E11H lysozyme variant had the following first four amino acid residues: MGKC.

A-2. Lysozyme expression and purification.

The lysozyme variants were over-expressed in *E. coli* using the following representative protocol. After transformation of the pET28-S90C lysozyme plasmid into BL21 DE3 *E. coli* cells, agar plates supplemented with kanamycin (40 μg/ml) were incubated overnight at 37 °C. The following day, a single transformant was used to inoculate 10 ml LB supplemented with kanamycin (40 μg/ml). The culture (10 ml) was used to inoculate 1 L of LB media. Cells were grown at 37 °C to an OD_{600} of 0.8, and induced with 1 mM IPTG. Following induction, the culture was grown at 30 °C for 4 h. Following expression, the culture was centrifuged at 6 krpm (4032 g) for 25 min at 4 °C, and the supernatant decanted. The cell pellet was resuspended in lysis buffer (20 mM Tris, 10 mM NaCl, pH 7.5) before cell lysis by sonication. The resultant cell culture was centrifuged at 16 krpm (17203 g) for 45 min at 4 °C. Subsequently, the supernatant was decanted, and filtered (0.45 μm). Next, the cell lysate was applied to a cation exchange column on a BioLogic DuoFlow FPLC. The purified lysozyme fractions were concentrated, filtered (0.45 μM, Millipore), and applied to a Superdex size-exclusion column. The S90C variant of lysozyme was eluted in PBS buffer (138 mM NaCl, 2.7 mM KCl, 8.1 mM Na_2HPO_4, 1.5 mM KH_2PO_4, pH 7.5). The homogeneity of lysozyme variants used in the electronic measurements was >95%, as estimated by SDS PAGE (Fig. S1).

A-3. Lysozyme substrate.

Peptidoglycan isolated from *Micrococcus luteus* was purchased from Sigma-Aldrich (St. Louis, MO) and used without further purification as a substrate to assay lysozyme

activity (*59*). The substrate was suspended to a final concentration of 25 μg/ml in PBS at pH 7.5. This concentration insures the presence of excess substrate for V_{max} conditions. After preparation, the peptidoglycan suspension was allowed to settle before use. Typically, 250 μL of supernatant solution was pipetted for application to the SWNT devices. This technique excluded the largest peptidoglycan fragments and aggregates. Additional data acquired using decreased substrate concentrations of 5 and 1 μg/ml were not detectably different from the results presented here.

A-4. SWNT synthesis and device fabrication.

SWNTs were grown by chemical vapor deposition (CVD) directly on 4" Si wafers, using techniques used successfully in past research (*17*). First, $Fe_{30}Mo_{84}$ catalyst nanoparticles were synthesized following previous reports (*60, 61*). A saturated solution of nanoparticles in ethanol was prepared, and then diluted 1:1000 in ethanol. Spin-coating the dilute solution onto a clean wafer surface at a low rate of 150 rpm provides a uniform and dilute coating of catalyst particles. CVD occurs in a custom-built 6" quartz tube furnace, and proceeds by a three-step process in which the catalytic clusters are first oxidized (700 °C; air), then reduced (940 °C; 520 sccm H_2 in 3000 sccm Ar), and finally exposed to a carbon feedstock (940 °C; 1000 sccm CH_4 + 520 sccm H_2 in 3000 sccm Ar). Our conditions result in an areal density of approximately 0.01 SWNTs/μm^2 and a SWNT diameter range of 1.1 – 1.6 nm. The reduced nanoparticles and resulting SWNTs were characterized by scanning electron microscopy (SEM, Philips XL-30 at 1 kV and 20 kV) and in air by noncontact atomic force microscopy (AFM, Pacific Nanotechnology Nano-R).

After CVD, wafers were next processed in a cleanroom environment. Optical lithography defined Ti electrodes on top of the randomly grown SWNTs with source-drain separations of 2 – 3 μm. We used an undercut bilayer resist (S1808 on top of LOR-A1, MicroChem) to improve liftoff and give clean interfaces. An electrostatic gate is defined by the degenerately doped wafer (p^{++} Si) and a 500 nm thermal oxide. Initial, wafer-scale electrical characterization identified about 30% of the SWNTs devices as metallic and 70% as semiconducting, consistent with the 1:2 ratio predicted theoretically. Individual devices were electrically probed, categorized, and finally imaged by noncontact atomic force microscopy to measure the SWNT diameter, confirm that only one SWNT is present in the device, and verify that each SWNT is free of particulates.

After initial characterization, each device undergoes a step of electron beam lithography. Devices were coated in electron beam resist (A3 PMMA, MicroChem) and patterned to expose an active SWNT channel 0.5 – 1.0 μm in length. This patterning ensured that the majority of the surface, including source and drain electrodes, remained protected from the test solution. The size of the PMMA window was also designed to maximize the probability of single-lysozyme attachments after protein conjugation. Devices were re-imaged by AFM after electron beam lithography to confirm that a SWNT was, in fact, exposed and that it remained free of particulates. The inset to Fig. 1B provides an example of the type of device accepted for further use.

A-5. Protein conjugation.

Devices were functionalized using the bifunctional linker molecule pyrene-maleimide. The pyrene group is commensurate with the SWNT sidewall and adheres to it

strongly via π-π stacking (*21*). The maleimide group can form stable thioether bonds with the free thiol of a cysteine sidechain (*62*). A solution of 1 mM *N*-(1-pyrenyl)maleimide (Sigam-Aldrich) in ethanol was prepared. Devices were soaked in solution for 30 min without agitation, and then washed with 0.1% Tween-20 (Acros Organics) in ethanol for 30 min with shaking to remove excess *N*-(1-pyrenyl)maleimide. After the first rinse, a second rinse was performed in a solution of 50% Tween-20 (0.1%) in ethanol and 50% phosphate buffer (20 mM Na_2HPO_4, pH 7) for 10 min with shaking to remove excess reagent. Then, the devices were rinsed under flowing de-ionized water for 5 min.

Next, a solution of a single cysteine variant of T4 lysozyme (54 μM) in phosphate buffer (20 mM Na_2HPO_4, pH 7) was prepared. At room temperature, devices were soaked in the lysozyme solution for 60 min without agitation. The devices were then washed with wash buffer (5 mM KCl, 10 mM Na_2HPO_4, 0.05% Tween-20, pH 7) for 30 min with shaking to remove unattached lysozyme. Finally, the devices were rinsed under flowing de-ionized water for 5 min. This rinsing protocol removed most but not all of the non-selectively adsorbed lysozyme from the SiO_2 surface. Harsher treatments to clean the surface were ruled out by the non-covalent nature of the pyrene-SWNT linkage, and cleaner surfaces could not be achieved without simultaneously affecting the yield of SWNT attachments, which already averages only 0.8 proteins per SWNT (i.e., one protein on 80% of devices). Mass spectrometry (MS) provided an assay for the optimization of the bioconjugation conditions with bulk quantities of the S90C variant of lysozyme (Fig. S2). Similar conditions were used for fabrication of the single lysozyme nanocircuits, as described above.

Following conjugation, devices were stored in PBS and not dried or imaged until the completion of measurements. Images such as Fig. 1B were therefore acquired after electrical characterization and probing with peptidoglycan substrate. Fig. S3A is an example device before polymethyl methacrylate (PMMA) coating, with a dashed line indicating the desired position of the PMMA window. Fig. S3B shows the same device after electron beam lithography and protein conjugation, now with two lysozyme proteins attached. Fig. S3C shows another device in which only one attachment occurred. AFM line cuts are provided in Fig. S3D for the three AFM images of (Figs. 1B, S3A, and S3B) and for three additional example devices. In each line cut, the pyrene-coated SWNTs appear to be 1.5 – 2.0 nm in height, while the attachment sites are 5 – 10 nm high. The difference is much more than the surface roughness along the rest of the SWNT, which we measure to be 0.2 – 0.4 nm. The range of heights observed at the lysozyme attachment site is consistent with the molecule's physical structure, especially considering that it can attach in different orientations around the SWNT circumference and that the images are acquired after drying the device.

It is noteworthy that our rinsing protocols maintain relatively clean surfaces throughout the experiments. The devices are processed by both optical and electron beam lithography, exposed to high concentration (0.24 M) salt solutions, soaked for long periods in solutions of both lysozyme and peptidoglycan, and yet the final surface fouling remains very low. Line cuts across the bare surfaces have peak-to-peak height ranges of 1.0 nm, and the rms surface roughnesses of the images in Fig. S3 are only 0.7 – 0.8 nm (including the SWNT topography but excluding the PMMA at the edges). A nonzero background of adsorbed lysozyme and/or peptidoglycan is unavoidable, but it compares

very favorably with similar work in this field (*6, 21, 53, 63*). In fact, the low background indicates that peptidoglycan is not precipitating onto the surface or being otherwise immobilized by strong surface interactions, an important feature since diffusional freedom is necessary for enzymatic processing to occur.

Finally, we find no evidence that protein adsorption far from the SWNT can affect the device behavior. The measured electrical currents are confined to the SWNT conductor and SiO_2-bound protein located 10 – 100 nm from the SWNT should be entirely screened by the PBS buffer electrolyte, which has a Debye length of 0.8 nm.

A-6. Electrical measurements.

All measurements described here were performed with the active portion of the device submerged in PBS buffer at the indicated pH values. The electrolyte potential was controlled by Pt counter and reference electrodes. The potential between the SWNT working electrode and the Pt reference was typically held at 0.0 V using a Keithley 2400 sourcemeter, though small values of 0.1 – 0.2 V were also used to maximize the slope dG/dV_g at the bias point. The source-drain bias was held at 100 mV, and the back gate at 0.0 V. Source-drain current was measured by a Keithley 428 preamplifer operating at 10^8 V/A gain and with a 40 μs rise time. Data was collected for at least 600 s at each fixed bias or pH value. Fig. 2 shows representative portions of these data sets, whereas Fig. 3 is an analysis of a full 600 s run.

Fig. 1D depicts a variation of the typical technique in that measurement was performed continuously during the addition of peptidoglycan substrate. Such a measurement is particularly challenging because two isolated fluids have independent temperatures and electrochemical potentials. Transients in the SWNT device current occur as thermal, chemical, and electrostatic equilibrium is achieved. Until the background noise level has been re-established, two level switching cannot be clearly distinguished.

We found that a pre-charging technique was most important for minimizing transients during fluid mixing and obtaining the resolution shown in Fig. 1D. First, a ~1 μL droplet of PBS buffer was manipulated into place over the SWNT device and maintained at a fixed potential. A much larger, 10-20 μL droplet of peptidoglycan solution was placed nearby on the PMMA/SiO_2 surface, allowing the solution to equilibriate thermally. Using a second set of Pt reference and counter electrodes mounted on a thumbscrew manipulator, we attempted to charge the larger droplet to the same potential as the smaller one. After beginning the electrical measurements, the two droplets were mechanically merged at t = 0 by dragging the larger droplet into contact with the smaller one using our reference electrode setup.

SOM Text

B. Electrical Fluctuations of Control Devices

B-1. Noise characterization of bare SWNTs.

A small percentage (<10%) of as-fabricated devices exhibited noise above normal values for SWNT devices (*64*), and particularly noisy devices even exhibit RTS switching at room temperature. This noise is due to SWNT defects or charge traps in the

underlying SiO_2 interacting with the surrounding environment (*65*). As-fabricated devices with substantial noise were discarded without further use.

Device noise was tested a second time after e-beam lithography defined the protective PMMA window. At this stage of the processing, extremely few devices exhibited higher noise levels or new RTS sources. Instead, the noise generally decreased, most probably due to passivation of the SWNT-metal electrode interfaces.

B-2. Response of bare SWNT to test analytes.

Control measurements tested for any dynamic response of the SWNT sidewall to the PBS buffer, or to the substrate molecules used to probe the dynamics of lysozyme. As shown in Fig. S4, unfunctionalized devices with PMMA windows showed no electronic signals that might be associated with dynamic interactions. No part of the noise power spectrum (DC – 10 kHz) was sensitive to the presence of substrate molecules.

After this initial test, the same SWNT devices were rinsed clean and conjugated to lysozyme as described above. With the added pyrene and lysozyme, devices that previously had no response showed two level fluctuations when probed with substrate.

B-3. Response of pyrene-coated SWNT to test analytes.

Additional control measurements tested for any dynamic response of the pyrene-coated SWNT sidewall. This control is particularly relevant because the final devices consist of a relatively high number of pyrene molecules coating the entire SWNT, whereas the lysozyme attachments are very dilute.

In the absence of lysozyme, pyrene-coated SWNTs were measured in PBS, and in the same PBS solutions of substrate molecules used to probe the dynamics of lysozyme. As shown in Fig. S5, pyrene-coated SWNTs showed no dynamic electronic response to the reagents. The same devices, after performing the lysozyme coupling reaction, exhibited two level fluctuations with substrate present.

One notable part of Figs. S4 and S5 is a small change in the DC current level. In general, the pyrene coating step tends to increase device conductance by 1-2 MΩ, whereas subsequent protein conjugation decreases the conductance. A cancellation is observed in Fig. S4, where a bare m-SWNT device has nearly the same current level after the combination of pyrene coating and protein conjugation. On the other hand, Fig. S5 compares a pyrene-coated device before and after protein conjugation, in which case an offset is clearly observed.

Note that Figs. S4 and S5 are collected from different devices that by coincidence have similar resistances of 2.0 – 2.5 MΩ.

B-4. Response of devices having inactive lysozyme variants.

The control experiments above provide compelling evidence that the two level fluctuations are specific to lysozyme-substrate interactions. Fluctuations are not caused by the SWNT device, by the pyrene coating, by the PBS buffer or substrate, or by the lysozyme itself in the absence of substrate.

To further test the source of the observed two-level fluctuations, we fabricated SWNT devices with the catalytically inactive variants of lysozyme T26E and E11H (*58*). The two mutated residues, Thr26 and Glu11, play key roles in the lysozyme mechanism for the catalysis of glycoside hydrolysis. The T26E variant produces a covalent adduct

with the peptidoglycan substrate, and thus provides a constitutively substrate-bound version of the lysozyme. The E11H variant is also catalytically inoperable, but does not form a covalent bond to the substrate.

Twelve devices were fabricated using the same methods described above, but using the T26E (eight devices) or E11H (four devices) variants. Upon the addition of substrate, all twelve devices prepared with an inactive lysozyme variant were equally quiet with and without substrate present, and no two level fluctuations were observed. Two examples of this are shown in Fig. S6. The absence of two level fluctuations in all 12 devices is markedly different from the 80% success rate we observe in devices that contain the active, S90C variant. AFM imaging of the devices indicated successful, single protein attachments with both T26E and E11H, and two example images are shown in Fig. S6D. The point mutations had no apparent effect on the attachment yield and the topographical AFM images were indistinguishable among the different variants.

The successful attachment and the absence of fluctuations together confirm that the observed signals are specific to the catalytic processing of lysozyme. This series of control experiments rules out the possibility that noncatalytic, merely electrostatic interactions between lysozyme and substrate might be causing the two level fluctuations.

As an aside, we note that the two inactive variants E11H and T26E are not easily distinguishable by our SWNT device technique, despite the fact that T26E permanently binds substrate and E11H does not. Our measurements suggest that an initial binding event by the T26E may cause a single, step-like increase in $I(t)$, but in general such isolated events are difficult to distinguish from the low frequency, 1/f fluctuations of the SWNT itself. All of the analysis described here is completed with the aid of a 10 Hz highpass filter to minimize this SWNT noise, and that filtering eliminates the only evidence of a difference between the E11H and the T26E variants.

B-5. Summary of device parameters for protein-conjugated SWNTs.

Of 20 SWNT devices conjugated with lysozyme and tested for activity, 18 showed the combination of fast RTS and slow RTS states described in the main text. Table S2 below summarizes important device parameters for five devices made from semiconductors (s-SWNTs) and five more made from metals (m-SWNTs). All of the data in the main text are for the m-SWNT device labeled #6. Here, we describe some of the noteworthy similarities and trends observed.

As-fabricated devices have a wide range of contact resistances and, subsequently, initial device resistances $R_{pristine}$. Table S2 includes a few examples of the minimum achievable contact resistance, which for our diameter SWNT is approximately 0.1 – 0.3 MΩ (*66-68*). We also tabulate the increase in DC resistance $\Delta R_{coating}$ that occurs after pyrene coating and protein conjugation. For the low resistance devices, functionalization adds 0.8 – 2.7 MΩ to the device resistance (at $V_g = 0$). Low resistance m-SWNTs and s-SWNTs both show the same range of changes, which indicates that simple electrostatic shifts of the $I(V_g)$ characteristics cannot be the primary mechanism responsible for the increase. Instead, we interpret $\Delta R_{coating}$ to be extra scattering along the SWNT sidewall caused by the attached molecules. Devices #4, 5, and 10 begin with anomalously high $R_{pristine}$ values and consequently increase resistance much more dramatically upon functionalization.

All of the devices in Table S2, as well as the control devices described above, do exhibit changes ΔI in their DC currents when the local environment is changed. In other words, the step in Fig. 1D at t = 0 is by no means unique, and similar results have been reported for a wide range of different analytes, using either pristine or functionalized SWNTs. Reviews of this phenomenon have been published recently (*34, 69*). What distinguishes the control devices from those in Table S2, however, is the presence of two level fluctuations that are the main focus of the text. No such fluctuations are observed in the control devices.

Table S2 tabulates mean values of the different current levels observed for each device. In particular, the current measured in PBS (I_{PBS}) can be compared to the high (I_{hi}) and low (I_{lo}) current values observed when the same device is switching. The general trend is for I_{lo} to be quite similar to I_{PBS}, which suggests that I_{lo} corresponds to the unbound configuration of lysozyme. I_{hi}, on the other hand, is substantially larger and is assigned to the bound substrate-lysozyme complex. We note that the inactive state described in the text is always inactive at the I_{lo} current level, proving that the inactive state is also an unbound configuration. While this assignment is likely to be correct, the trend is not without apparent exceptions. Four of the m-SWNT devices have $I_{lo} \approx I_{PBS}$, but in device #9 both currents I_{hi} and I_{lo} are substantially higher than would be expected from R_{coated}. Continuous measurements prove that R_{coated} is a very poor benchmark, because its value varies in time and is dependent on surface charge transfer and the liquid electrolyte potential, strongly so for s-SWNT devices.

The most reliable parameter, we believe, is the relative difference $\Delta I_{RTS} = (I_{hi} - I_{lo}) / I_{lo}$, because ΔI_{RTS} is insensitive to slowly varying processes. Background removal techniques shown in Figs. 2A and B are very effective for the statistical analysis of ΔI_{RTS}. This reliability leads to the very uniform values of ΔV_g that are discussed in detail in the main text. DC changes in current are, by comparison, extremely difficult to attribute to any particular source. This reliability issue underscores a main difficulty in using nanoscale devices as DC chemical or biological sensors, and their promise for monitoring dynamic processes as reported here.

Because of this high degree of reliability, it is particularly noteworthy that ΔI has the same distribution of values for both fast RTS and slow RTS oscillations. For the proposed electrostatic transduction, this constancy indicates that the enzyme undergoes a similar range of conformational motions during both types of oscillation. Indeed, FRET proves that a lysozyme's range of mechanical motion is the same for both types of activity (*37, 40, 42*).

B-6. A qualitative comparison of covalent and noncovalent attachment techniques

Lysozyme sensing experiments were accomplished as early as 2006 with very promising preliminary results. The initial work followed our success introducing point defects in SWNTs (*17*), modifying those defects to include carboxylic groups (*70*), and then conjugating amines directly to those groups using EDC/NHS zero-length linkages (*71*). Using this multi-step protocol, individual lysozyme molecules were covalently linked to SWNT sidewalls. Electrical measurements clearly observed peptidoglycan-induced, time-varying fluctuations having a broad spectral peak in the 200 – 400 Hz range, and these results were reported at various conferences and in two dissertations (*72, 73*).

However, subsequent investigation found these early devices to be too idiosynchratic for reliable analysis.

First, the covalent attachment scheme results in much lower device yield than the noncovalent scheme reported here. When performed with the utmost care, the introduction of carboxylates and the covalent attachment of lysozyme has been accomplished with 50% yield. Yields of 10 – 25% are more typical, however, complicating efforts to perform reliable control measurements. By comparison, the noncovalent technique described here requires minimal modification of the SWNT, so that very few devices are lost as open circuits at any point in the functionalization process.

Second, devices with carboxylate defects tend to introduce more resistance and more noise than other types of SWNT defects, and they are much more resistive and noisy than unmodified SWNTs. The covalently-linked devices therefore have small mean currents and large peak-to-peak noise. This combination severely limits the ability to observe small amplitude, two-level switching, much less to accumulate reliable statistics. Using the covalent functionalization scheme, two level switching events were not always distinguishable, even when the average power spectrum indicated the presence of fluctuations.

Third, carboxylate defects open the SWNT lattice and provide multiple chemical pathways for further SWNT oxidation. In practice, we find that SWNTs with carboxylates are highly likely to increase in resistance over time, ultimately becoming open circuits after extensive measurement. Noncovalently modified SWNTs, on the other hand, behave more like pristine SWNTs in that they can be measured indefinitely when standard static discharge precautions are observed.

Ultimately, our work to understand the limitations of covalent lysozyme attachments led us to the noncovalent scheme described here. In the present work, the yield of well-behaved, long-lived devices has exceeded 90%. Every device prepared with a lysozyme has generated clear two-level switching, and this reliability has greatly improved our confidence in the control measurements using inactive lysozyme variants. Furthermore, the pyrene-maleimide linkage is very general and is immediately applicable to other biomolecules of interest. Experimentally (*19, 20*) and theoretically (*54*), the covalent attachment scheme is promising and conceptually appealing, but we believe the noncovalent scheme may be more readily reproduced by others in the field.

C. Additional Analysis of Electrical Fluctuations

C-1. Summary of device parameters for protein-conjugated SWNTs.

Analysis of the time-scales for the lysozyme tethered to the nanocircuit can provide insights into the underlying chemistry. As subcomponents of the turnover rates, τ_{lo} and τ_{hi} have two important characteristics. First, τ_{lo} was about 20 times greater during effective catalytic processing than during the faster, nonproductive binding events. Second, the ratio τ_{hi}/τ_{lo} determines a thermodynamic energy ΔE that was 1.1 kcal/mol greater during catalytic processing than during nonproductive binding (Table 1). The rate-determining step for the reaction catalyzed by lysozyme is likely the formation of an oxocarbenium-like transition state, which requires acid-base catalysis by active site residues (*35, 36, 74*). Successful formation of the transition state requires additional

energy ΔE as well as sufficient time τ_{lo} for the substrate to shift within the active site. In our interpretation, τ_{lo} results from the open conformation of the enzyme active site. τ_{hi}, on the other hand, reflects a submillisecond state that corresponds to the closed conformation of lysozyme. FRET experiments observe that hinge closure occurs during both productive and nonproductive binding (*42*). In the catalytically productive case (slow RTS), τ_{hi} is two to four times greater than it does during nonproductive binding (fast RTS). The longer duration correlates with the formation of the activated enzyme-substrate complex and subsequent cleavage of the substrate. At non-optimal pH values, the enzyme spent less time in the activated complex or closed conformation (Table 1).

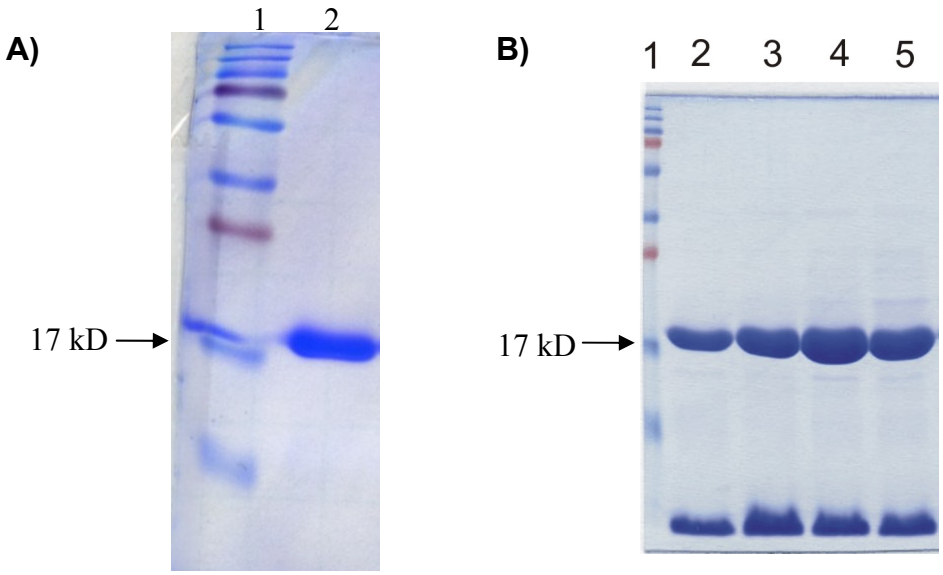

Figure S1. Expression and purification of T4 lysozyme. (A) The S90C variant of lysozyme. This 15% SDS-PAGE gel provides an illustrative example of the homogeneity of over-expressed lysozyme variants. Following cation-exchange and size exclusion chromatography, lysozyme migrates as expected for a 18.6 kD protein (lane 2). Lane 1 is the PageRuler Plus Prestained Protein Ladder (Fermentas). **(B) The E11H variant of lysozyme.** This SDS-PAGE of fractions following both size exclusion chromatography and cation-exchange chromatography demonstrates the effectiveness of the protein purification protocols. The E11H variant of lysozyme in lanes 2-5 was concentrated before bioconjugation to the SWNT nanocircuits.

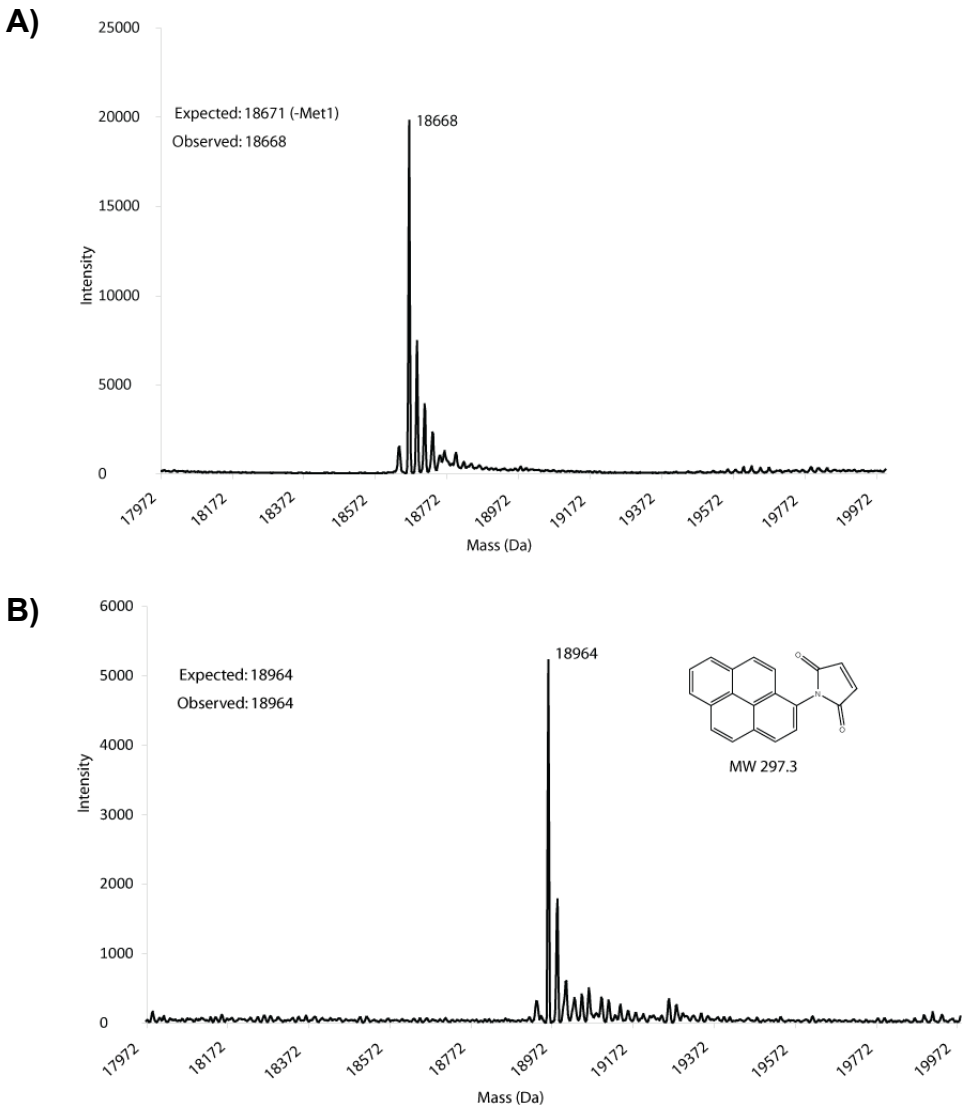

Figure S2. ESI-MS data illustrating pyrene maleimide linker conjugation to lysozyme. In this experiment, lysozyme and *N*-(1-pyrene)maleimide were mixed at equal molar ratios in PBS (pH 7.5), and incubated at room temperature for 20 min prior to ESI-MS analysis. **(A)** The peak at 18668 Da represents the S90C variant of lysozyme prior to the bioconjugation reaction with the N-terminal methionine residue proteolytically removed during protein over-expression and/or isolation. **(B)** Following reaction with *N*-(1-pyrene)maleimide (inset), a new peak at 18964 Da is observed, and its mass is consistent with the S90C variant of lysozyme covalently conjugated to the pyrene maleimide linker. The unmodified protein cannot be detected by MS after the reaction, which suggests a high efficiency bioconjugation reaction.

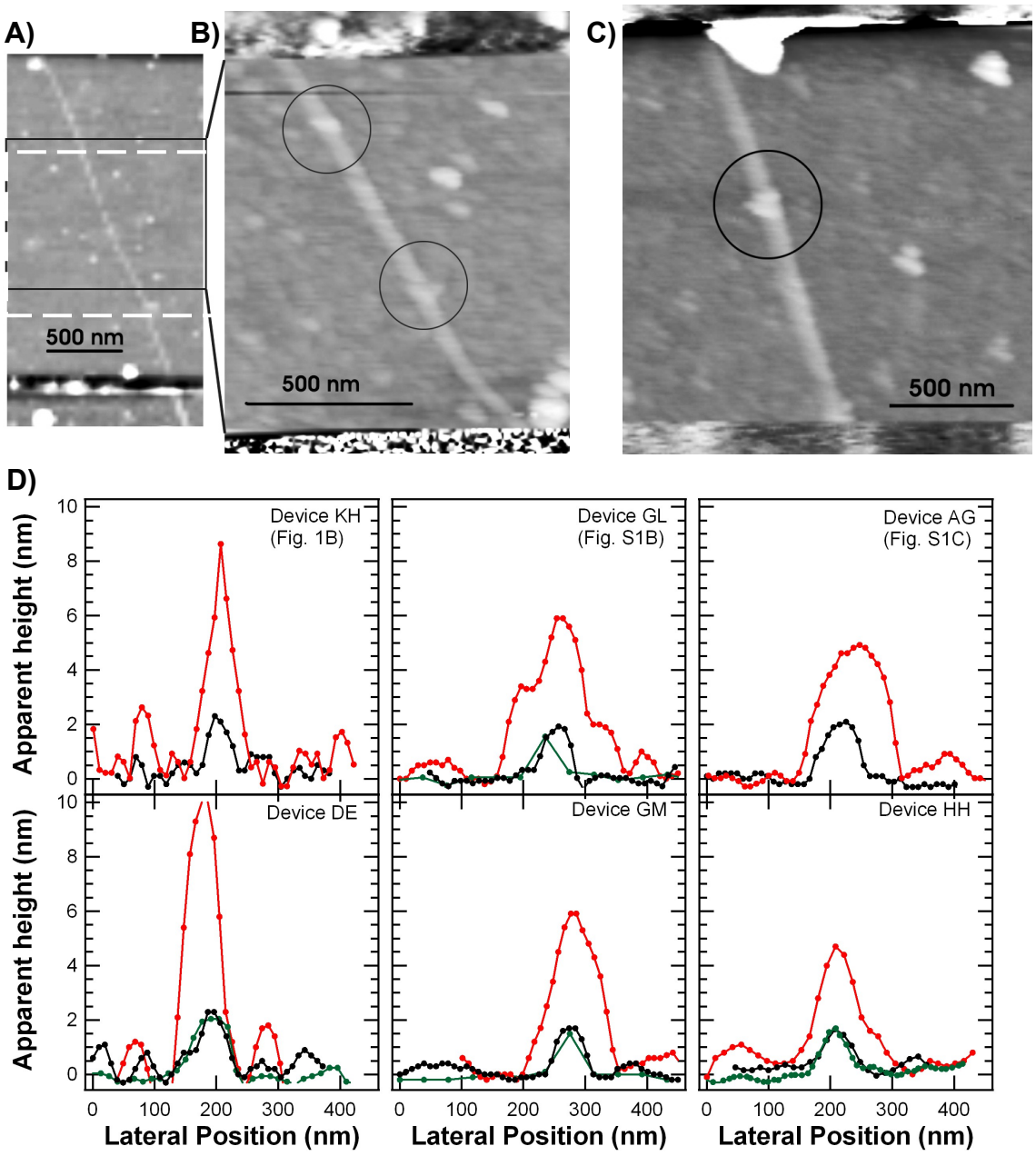

Figure S3. Additional examples of lysozyme device fabrication. (A) AFM image of a bare SWNT device with the target position of the PMMA window indicated (dashed box). (B) A higher magnification image of the same device after bioconjugation, which resulted in two lysozyme attachments (grey circles). Note the larger scale bar, and that the top and bottom edges of the image now correspond to the protective PMMA rather than to metal electrodes. (C) A device with a single lysozyme attachment. (D) AFM line profiles for 6 different devices, including three shown here and in Fig. 1B. Three lines in each image correspond to height profiles taken across the lysozyme attachment (red), pyrene-coated SWNT (black), and pristine SWNT (green).

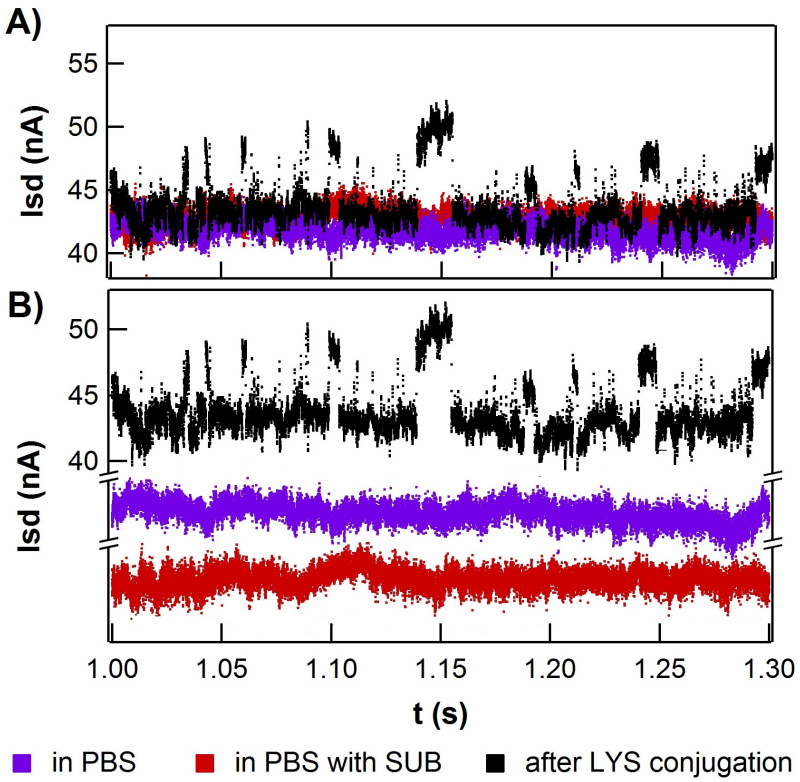

Figure S4. Bare SWNT control experiments. (A) Plot shows typical *I(t)* fluctuations for a bare SWNT measured in PBS buffer, without substrate (purple) or with substrate (red) present. Subsequently, the same device is functionalized with pyrene and lysozyme, and then remeasured in PBS with substrate (black data). (B) The same data, offset from the functional device for clarity.

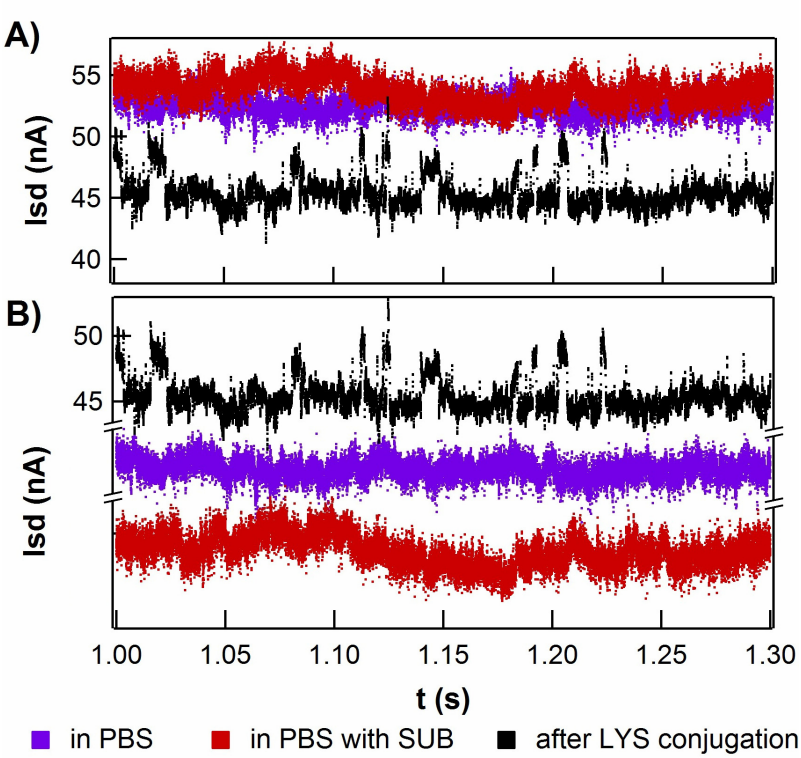

Figure S5. Pyrene-coated SWNT control experiments. (A) Plot shows typical I(t) fluctuations for a pyrene-coated SWNT measured in PBS buffer, without substrate (purple) or with substrate (red) present. Subsequently, the lysozyme coupling reaction is performed on the same device, and then it is remeasured in PBS with substrate (black data). Note that the lysozyme coupling reaction decreases the device conductance by approximately 10%. (B) The same data, offset from the functional device for clarity.

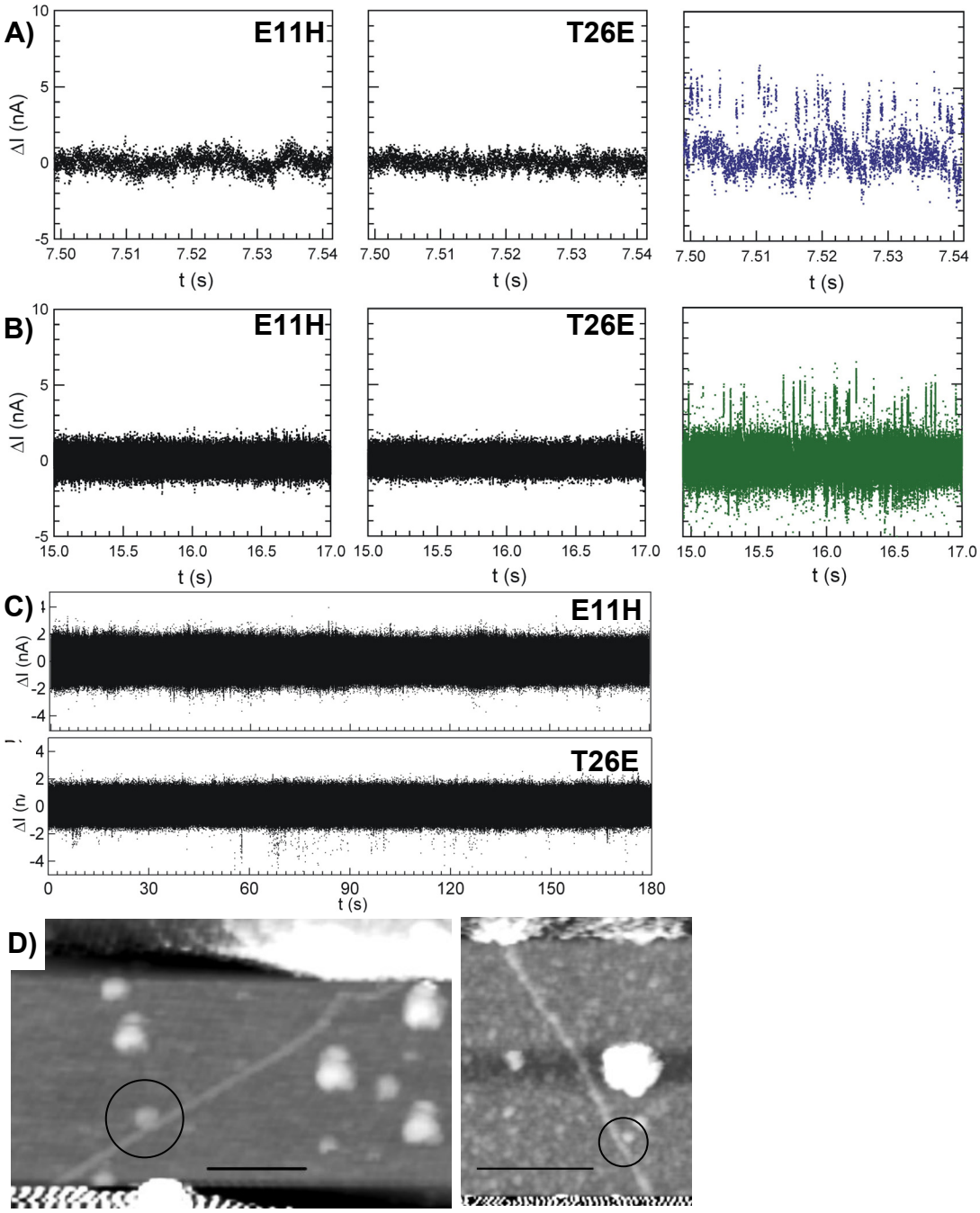

Figure S6. Control experiments with catalytically inactive lysozyme variants. The E11H and T26E lysozyme variants show no two-level switching when inspected over (A) 40 ms, (B) 2 s, or (C) 180 s intervals. For a direct comparison, Figs. 2C and 2D with comparable time-scales are reproduced here to show data from the active lysozyme variant discussed in the text. The E11H variant can not bind substrate in its active site, and the T26E variant forms a long-lived, covalent bond to substrate with no catalytic activity. Note that when no switching is present, the experimental variable ΔI does not distinguish whether the enzyme is in its open or closed conformation. (D) Example AFM images of 2 of the 12 devices fabricated with inactive variants. Scale bars are 500 nm.

Oligonucleotide	Sequence (5'-3')	Purpose
P1-ForNormal	CATGCCATGGGGAAAAATATATTT GAAATGTTACGTATAGATGAAGG	Amplification and NcoI digestion
P2-RevSC90	GCGCGACGAACCGCATCAAGACA ATCATAAACCGGTTTTAATTTAG	S90C mutation
P3-ForSC90	CTAAATTAAAACCGGTTTATGATT GTCTTGATGCGGTTCGTCGCGC	S90C mutation
P4-RevNormal	CCG CTC GAG CGG TCA TAG ATT TTT ATA CGC GTC CCA AGT GCC	Amplification and XhoI digestion
P4-Rev6xH	CTTGGGACGCGTATAAAAATCTAGAAAA TCTGTATTTTCAAGGTCCGCTCGAGCGG	Amplification to install His-tag and XhoI digestion
P2-RevT26E	GTAAGCAAATGACCGATGCCA ATTTCGTAATAGCCTTCTGTGTC	T26E mutation
P3-ForT26E	GACACAGAAGGCTATTACGAA ATTGGCATCGGTCATTTGCTTAC	T26E mutation
E11H-For	GAAATGTTACGTATAGATCATGGT CTTAGACTTAAAATCTATAAAGAC	E11H mutation
E11H-Rev	GTCTTTATAGATTTTAAGTCTAAG ACCATGATCTATACGTAACATTTC	E11H mutation

Table S1. Oligonucleotides used for the mutagenesis of lysozyme.

#	Type	$R_{pristine}$ (MΩ)	R_{coated} (MΩ)	$\Delta R_{coating}$ (MΩ)	I_{PBS} (nA)	I_{lo} (nA)	I_{hi} (nA)	ΔI_{RTS} (%)	dI/dV_g (%/V)	ΔV_g (V) calc
1	s-SWNT	0.28	1.2	0.9	36*	40*	48*	+20%	95	0.21
2	s-SWNT	0.38	1.5	1.1	87	103	122	+18%	88	0.21
3	s-SWNT	0.34	3.0	2.7	5.65	7	10.5	+50%	266	0.19
4	s-SWNT	17.6	56	38	2.5	2.8	2.9	+4%	20	0.20
5	s-SWNT	26.1	40	14	7.0	7.2	8.2	+14%	70	0.20
6	m-SWNT	0.10	1.4	1.3	78	80	82	+3%	18	0.16
7	m-SWNT	0.30	2.0	1.7	54	54	58	+7%	46	0.15
8	m-SWNT	0.35	2.6	2.2	42	45	50	+10%	54	0.19
9	m-SWNT	1.0	1.8	0.8	55	80	83	+4%	21	0.18
10	m-SWNT	3.0	30	27.1	3.5	3.3	4.9	+47%	235	0.20

*Measured at V_{sd} = 50 mV.

Table S2. SWNT-Lysozyme device characteristics.